Physics of Plasmas

A polar direct drive liquid deuterium–tritium wetted foam target concept for inertial confinement fusion

Cite as: Phys. Plasmas **28**, 122704 (2021); https://doi.org/10.1063/5.0062590
Submitted: 06 July 2021 • Accepted: 13 October 2021 • Published Online: 02 December 2021

R. E. Olson, M. J. Schmitt, B. M. Haines, et al.

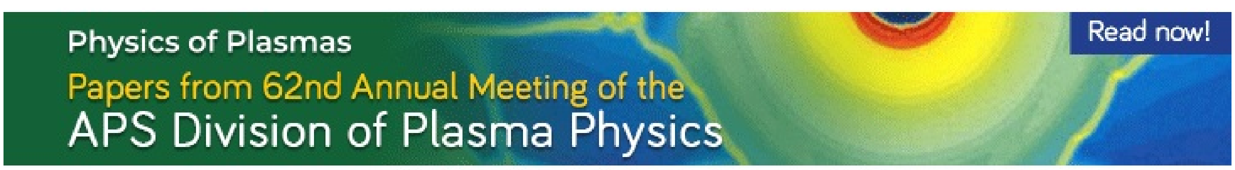

Physics of Plasmas ARTICLE scitation.org/journal/php

A polar direct drive liquid deuterium–tritium wetted foam target concept for inertial confinement fusion

Cite as: Phys. Plasmas **28**, 122704 (2021); doi: 10.1063/5.0062590
Submitted: 6 July 2021 · Accepted: 13 October 2021 ·
Published Online: 2 December 2021

R. E. Olson,[1,a)] M. J. Schmitt,[1] B. M. Haines,[1] G. E. Kemp,[2] C. B. Yeamans,[2] B. E. Blue,[2] D. W. Schmidt,[1] A. Haid,[3] M. Farrell,[3] P. A. Bradley,[1] H. F. Robey,[1] and R. J. Leeper[1]

AFFILIATIONS

[1]Los Alamos National Laboratory, Los Alamos, New Mexico 87185, USA
[2]Lawrence Livermore National Laboratory Livermore, California 94551, USA
[3]General Atomics, San Diego, California 92186, USA

[a)]Author to whom correspondence should be addressed: reolson@lanl.gov

ABSTRACT

We propose a new approach to inertial confinement fusion (ICF) that could potentially lead to ignition and propagating thermonuclear burn at the National Ignition Facility (NIF). The proposal is based upon a combination of two concepts, referred to as polar direct drive and liquid deuterium–tritium wetted foam capsules. With this new concept, 2D radiation hydrodynamic simulations indicate that ICF ignition and propagating thermonuclear burn are possible with the laser power and energy capabilities available today on the NIF.

I. INTRODUCTION AND BACKGROUND

Achieving ignition and propagating thermonuclear burn via inertial confinement fusion (ICF) is one of the primary goals of the U.S. Department of Energy research at the National Ignition Facility (NIF).[1] Since its completion in 2009, NIF experiments have been devoted primarily to the indirect drive ICF concept.[2] After 12 years of slow, but steady progress, indirect drive experiments at NIF have recently come close to demonstrating ignition.[3] It is now timely to begin exploring a path forward to higher yields and significant fusion gain. The original vision of the NIF was to explore all approaches to laser-driven ICF. In the present paper, we explore an alternative ICF concept that can potentially achieve much higher thermonuclear yields at the NIF. The approach involves a combination of two concepts, referred to as polar direct drive (PDD)[4] and liquid deuterium–tritium (DT) wetted foam (WF) capsules.[5] Separately, both concepts have been successfully demonstrated in NIF experiments.[6,7] Here, we propose that the two concepts be combined to create a new class of ICF targets that can potentially lead to high thermonuclear yields and significant fusion gain using a capsule drive that is within the laser power and energy capabilities available today at the NIF.

The baseline indirect drive DT ice layer ICF capsule design[8] requires a hot spot convergence ratio CR > 30 (hot spot convergence ratio is defined as the ratio of the initial radius of the DT gas, R_i, to the radius of the hot spot, CR $= R_i/R_{hs}$). High CR implosions require an exceptionally high degree of drive symmetry. For *indirect drive*, good drive symmetry requires a large hohlraum (compared with the capsule size), which results in a poor efficiency ($\sim$20% or less) in converting laser energy to capsule absorbed energy. In laser *direct drive*, the laser energy can be absorbed by a larger capsule with a higher overall efficiency. However, the NIF laser beam geometry is designed for heating indirect drive ICF hohlraums. As such, the NIF laser beams enter the vacuum chamber at angles near the poles in order to heat a cylindrical hohlraum aligned along the vertical axis of the target chamber. Direct illumination of a capsule at NIF requires a repointing of the beams toward the equator in a process referred to as polar direct drive (PDD).[4] The symmetry of the NIF PDD configuration may not be adequate for driving high convergence (CR > 20) implosions, but sufficient symmetry has been demonstrated for modest CR implosions of DT gas-filled capsules using PDD. Recently, these PDD implosions have achieved a very high efficiency conversion of NIF laser energy to thermonuclear fusion output, with neutron yields $\sim 10^{16}$.[6]

The current PDD neutron yields may be close to the limit that can be obtained with DT gas-filled capsules at the NIF. The initial idea of the current proposal was to increase the neutron yield further ($>10^{17}$) by adding a liquid DT layer to the inner surface of a PDD capsule. The Los Alamos National Laboratory (LANL) and Lawrence Livermore National Laboratory (LLNL) authors of this paper, together with other researchers at LLNL and University of Rochester Laboratory for Laser Energetics (LLE), used several different radiation hydrodynamic codes, which all indicated that, in 1D simulations, the simple PDD liquid DT layer concept would have the potential to produce thermonuclear yields in the range of 10–100 MJ using drives well within the laser power and energy capabilities of the NIF. Preliminary 1D results were discussed in Ref. 9, and a year later, more detailed 1D and 2D simulations of the initial PDD liquid layer concept, including a DT+CH (Carbon Hydrogen) wetted foam layer with mixed equation of state (EOS) were presented.[10] However, it was found that the initial concept produced high yields in 1D, but would not ignite in 2D simulations. As discussed in Ref. 10, the feedthrough of low-mode PDD drive asymmetries during the compression burn phase presented major challenges in the 2D simulations.

It is known from previous indirect drive wetted foam design simulations[11] and associated experiments[7,12,13] that a DT+CH mixed EOS must be used for accurate modeling of the wetted foam layer. A mixed EOS is less compressible than a pure DT EOS and that was found to be an important aspect in the modeling of the previous NIF wetted foam implosion experiments. A direct comparison showing the compressibility effect in 1D simulations of PDD liquid layer implosions using pure DT liquid layers and wetted foam layers was included in Ref. 10. Another important aspect to consider is that, at ignition, a small amount of carbon in the hot spot will increase the ideal ignition temperature. For example, a 25 mg/cm^3 CH foam wetted with liquid DT contains ~2% atomic fraction of carbon. A plot of ideal ignition temperature vs atomic fraction of carbon in the hot spot is shown in Ref. 14. Depending upon the vapor density and corresponding vapor hot spot mass fraction, the plot indicates that, with a 25 mg/cm^3 CH foam wetted with liquid DT, ideal ignition temperature might be increased to as high as 5.2 keV. An additional effect of the foam is that it delays ignition and burn propagation. As was shown in the 1D comparison simulations of the initial PDD liquid layer concept,[10] with the DT+CH mixed EOS (25 mg/cm^3 wetted foam), ignition is delayed and burn propagation is slowed compared with the pure DT simulation. Yet, both 1D simulations ignited and had high yields (100 MJ for pure DT and 71 MJ for the wetted foam). The basic problem was that this simple initial PDD liquid layer design would not ignite in the 2D simulations in Ref. 10, and a new design would be required. It should be mentioned that, during this same time frame, 1D simulations of the initial liquid layer target concept were also explored in an independent study in the UK[15] (with one coauthor, Haines, in common with the Refs. 9 and 10 LANL/LLNL study). Unlike the LANL/LLNL work that focused on NIF, the UK study considered a wide range of potential capsule sizes and laser energies for the initial PDD liquid layer concept. Yet, unlike the studies described in Ref. 10, the 1D simulations in Ref. 15 did not include a DT+CH wetted foam layer with mixed EOS, and 2D simulations were not attempted in Ref. 15.

II. THE POLAR DIRECT DRIVE WETTED FOAM (PDD-WF) TARGET CONCEPT

After the computational studies discussed above, a more sophisticated target design, the polar direct drive wetted foam (PDD-WF) design, was developed. Unlike the simple initial liquid layer concept, the PDD-WF design has been found to readily ignite in 2D simulations. The capsule in this design harkens back to the 1987 Sacks and Darling concept,[5] where the outer portion of the liquid DT wetted foam is an efficient ablator and the inner portion is the fuel layer. The low foam density reduces both the initial aspect ratio and the in-flight aspect ratio (IFAR), alleviates the effects of instability growth, and inhibits the feedthrough of low-mode asymmetries. Furthermore, as was discussed in Refs. 7, 12, and 14, the cryogenic fielding temperature controls the central DT vapor density and provides a technique for controlling implosion convergence in the range of $10 < CR < 18$.

The new PDD-WF concept is based on the synthesis of the five following ideas: (1) laser PDD with small beams for enhanced energy coupling to the target; (2) a low peak laser intensity at the absorption surface to suppress laser-plasma instabilities (LPI); (3) the use of emergent 3D printing fabrication for "designer" targets/foams; (4) a liquid DT layer to tune hot spot convergence ratio in a modest range that is not possible with a DT ice layer; and (5) the use of a thick liquid DT ablator layer to increase hydrodynamic stability through decreased IFAR. A pie diagram of the PDD-WF target is shown in Fig. 1. A key feature is that the outer portion of the liquid DT wetted foam is the ablator, and the inner portion serves as the fuel layer. The hot spot is initiated in the central DT vapor. A thin CH skin is required on the outer surface to contain the liquid DT. Wetted foam was proposed as an efficient direct drive ablator in Ref. 5, and 20 years later, the efficiency was confirmed with more modern computational simulations.[16] The use of wetted foam as both ablator and fuel layer provides a flexible design parameter that can be used to control the IFAR of the implosion. By varying the foam density and shell thickness, the thickness of the imploding wetted foam shell can be controlled to help reduce the deleterious effects of instability growth and hot spot mix. The cryogenic fielding temperature of the liquid DT layer controls the central DT vapor density and, hence, provides a demonstrated ability to control implosion convergence in the range of $10 < CR < 18$. This experimental concept requires the use of a DT liquid layer (as opposed to a DT ice layer) because the vapor density below the DT triple point is limited to <0.6 mg/cm^3, producing a high convergence implosion for DT ice. The indirect drive national ignition campaign (NIC) point design[8] employed a DT ice layer that had a vapor density of 0.3 mg/cm^3, with a hot spot CR of 35. In contrast, DT liquid layers can exist with much higher central region vapor densities, which enable

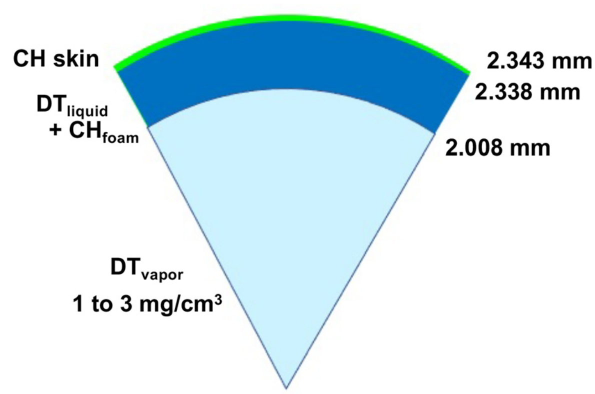

FIG. 1. The PDD-WF target concept with dimensions used in the 2D simulations.

the reduced convergence DT layer implosions that we require. NIF experimental demonstrations of the ability to control the convergence of DT liquid layer implosions are described in Refs. 7, 12, and 13.

The advantages of reduced convergence implosions to suppress hydrodynamic instabilities and mix are well known and discussed, for example, in Refs. 11, 13, and 14. It is generally acknowledged that the predictive capability of hot spot formation can be robust and 1D-like for a relatively low CR hot spot, but will become less reliable as hot spot CR exceeds 15. Computational simulations of wetted foam targets have shown that the ratio of 2D to 1D yield is in the range of 95%–100% for low convergence implosions (even in the presence of very large low-mode capsule asymmetries[13]) but that the 2D/1D yield ratio is significantly degraded for higher convergence ratios.[11,13,15,17] In addition, 3D simulations indicate that 3D effects (e.g., fill tube) become important as the CR increases, with performance degradations increasing significantly as CR increases beyond 15.[18] In both gas capsule and wetted foam layer experiments at NIF, the experience has been that 2D simulations have good predictive capability for implosion experiments with CR of about 15 or less.[7,12,13]

The PDD-WF design is driven by a NIF laser pulse that employs 192 narrow beams pointed in a polar direct drive laser configuration as shown in Fig. 2. The NIF's laser beam quads are located on the target chamber walls in four polar angle rings at 23.5°, 30°, 44.5°, and 50° from each pole and contain 4, 4, 8, and 8 beam quads, respectively, equally spaced longitudinally in phi around the target chamber. For this design, each individual beam is pointed at a unique location on the capsule surface. The upper and lower pairs of beams from each quad are split to point at different polar angle positions on the capsule resulting in eight different polar rings of beams on the capsule. These angles were adjusted to minimize the variation in velocity of the shell with respect to polar angle as measured prior to shell deceleration. The polar angles for the sub-rings of beams are 12.5°, 30°, 37.5°, 41.5°, 54°, 65.5°, 79°, and 85.5°. It is also assumed that the beam pairs are also split in longitudinal angle phi to achieve equal spacing of the beams from each sub-ring on the capsule surface. However, since these are 2D simulations, phi dependence on the shell dynamics is not included in these results.

The current phase plates on NIF produce focal spots of roughly 1 mm in diameter. However, NIF allows defocusing of each beam by up to 35 mm to produce beams of roughly 2 mm in width at the capsule surface. This larger beam size, in combination with the optimized spacing of the beams, produces a drive uniformity that can drive the capsule with sub-1% velocity uniformity from equator to pole even though the beam-to-capsule ratio here is about 0.4. These smaller beams increase the laser coupling to the target and reduce seeding of cross beam energy transfer (CBET)[19–22] energy scatter from the capsule. The baseline design assumes equal drive power on all 192 beams. Any observed P_2 asymmetry in the design is then tuned out by adjusting the power in the 23.5° beams. Such asymmetries can arise when changing the material properties of the shell. For the design described here, an 8% increase in the power of the 23.5° beams was used. The maximum drive power during the laser pulse was 230 TW and the integrated energy in the pulse was 1.4 MJ, significantly lower than the current energy available in NIF. The laser pulse shape is shown in Fig. 3. The early time "foot" of the laser pulse creates a blow-off plasma that is used to set the position of the laser absorption region beyond the original capsule radius. As will be shown in Sec. III, radiation hydrodynamic simulations indicate that the laser absorption region remains at a diameter of about 5–6 mm throughout the laser pulse. This results in a low average intensity ($<$250 TW/cm^2) in the laser absorption region. In previous NIF experiments with a similar PDD pointing scheme and spot size, capsules have been imploded successfully with a demonstrated $\sim$99% laser absorption when the peak intensity in the laser absorption region is kept below 250 TW/cm^2.[23,24] A paper is currently in preparation to provide details and compare CBET simulations to the recent large capsule, low-intensity, and low-backscatter NIF results. Based on these experimental results, the PDD-WF design seeks to avoid the LPI and CBET issues by employing a peak intensity in the laser absorption region that remains well below 250 TW/cm^2 throughout the laser pulse.

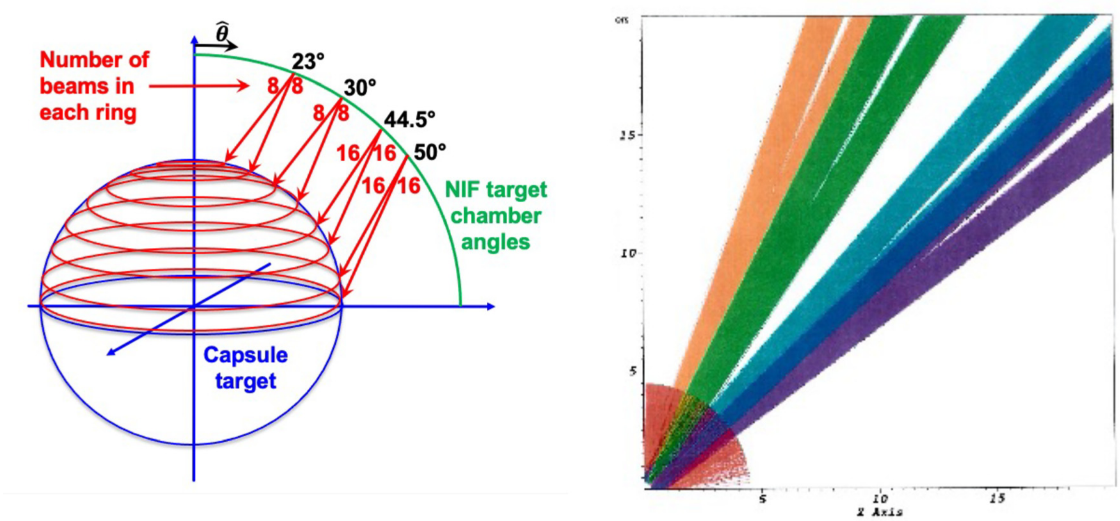

FIG. 2. Illustration of the NIF split quad laser pointing geometry used in the 2D simulations.

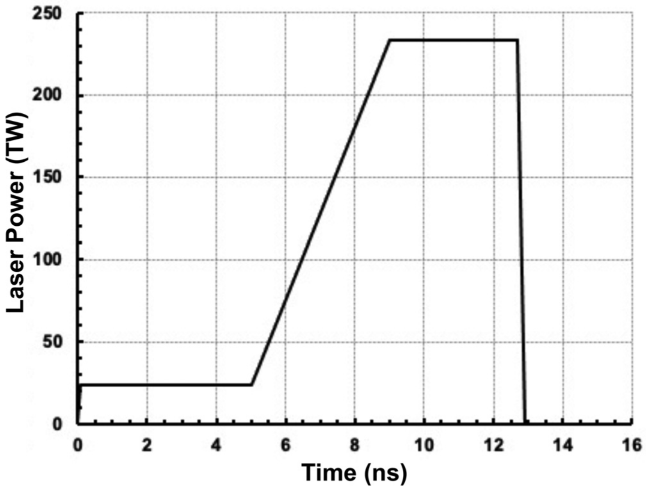

FIG. 3. The laser pulse shape used as input in the 2D simulations.

The PDD-WF targets are made possible using an emergent technology for the one-piece integrated 3D printing of the foam shell, outer skin, and fill tube entrance hole. Such an additive manufacturing fabrication technique has been used to produce a 3D printed prototype of a PDD-WF capsule (Fig. 4). The prototype is based upon the PDD-WF capsule specifications and dimensions shown in Fig. 1. A photograph of the prototype capsule is shown in Fig. 4(a). Figure 4(b) is a full diameter tomographic image of the capsule. The blue region is the foam (or "lattice") shell (density is 20 mg/cm^3), and the green is the outer CH skin. The tomography data can be evaluated for uniformity of the thickness, roundness, and density of the lattice and skin. Figure 4(c) is a radiograph showing details of the fill tube region. The CH skin extends halfway into the fill tube hole so that the fill tube can be attached while leaving enough space for the liquid DT to flow into the CH foam. The method used to 3D print is called "2 photon polymerization" (2PP).[25] General Atomics (GA) develops and constructs custom 2PP systems that allow for the tailoring of the technology to target fabrication, among other things. Examples of recent GA 3D printed 2PP for targets (microtubes, parabolic cones) are discussed in Refs. 26 and 27. The prototype target shown in Fig. 4 was printed with a 2PP process that resulted in a foam shell having a composition of approximately $C_{11}H_{12}O_3$. However, there are modest advantages to reducing the oxygen content in the foam, and efforts are under way to develop a process that can print a pure CH foam shell.

The PDD-WF capsules must be fielded at temperatures in the range of 20–27°K so that liquid DT can wet the lattice region of the shell. In a recent experiment at the NIF, a large PDD gas capsule was cooled to a fielding temperature of ~40°K using a copper fill tube. However, it has yet to be demonstrated that a PDD-WF capsule can be fielded on NIF at the cooler liquid DT temperature and maintained at this temperature until shot time using the copper fill tube technique. Should issues arise, a more complex fielding geometry involving a retracting thermal shield (similar to what has been done on Omega[19]) may be required to field this target.

III. COMPUTATIONAL SIMULATIONS OF THE PDD-WF TARGET CONCEPT

The 2D computational simulations discussed in the present paper were performed at LANL with the HYDRA radiation hydrodynamics code.[28] The 2D simulations utilized HYDRA's 3D laser ray trace and inverse Bremsstrahlung energy deposition package. Simulations assumed 300 laser rays per beam with the individual beams having an f-number of 22 with focal positions located 35 mm past target chamber center. Flux limited heat conduction, multi-group radiation diffusion, and opacities from the LLNL opacity server were used in the simulations. The Livermore equation of state (LEOS) tables were used with a mixed EOS model employed for the DT+CH mixture in the wetted foam region. The thermonuclear burn model includes fusion product transport and energy deposition. Typically, a hydrodynamic grid spatial resolution of 1 degree was used in the polar angle direction for most of the concept evaluation simulations, but a few simulations using a 0.5° angle were also done. For reasons previously discussed, peak intensities in the laser absorption region were kept below 250 TW/cm^2. Because of the lack of significant scattered power seen in previous large capsule NIF experiments driven at these low intensities, and the fact that the quarter critical radius (near where CBET interactions occur) does not shrink below the original capsule radius during the laser pulse, no laser plasma instability (LPI) loss mechanisms were included in these design simulations. However, should CBET effects become problematic, techniques for their suppression[20,21] and asymmetry compensation exist[20] and could be employed if needed.

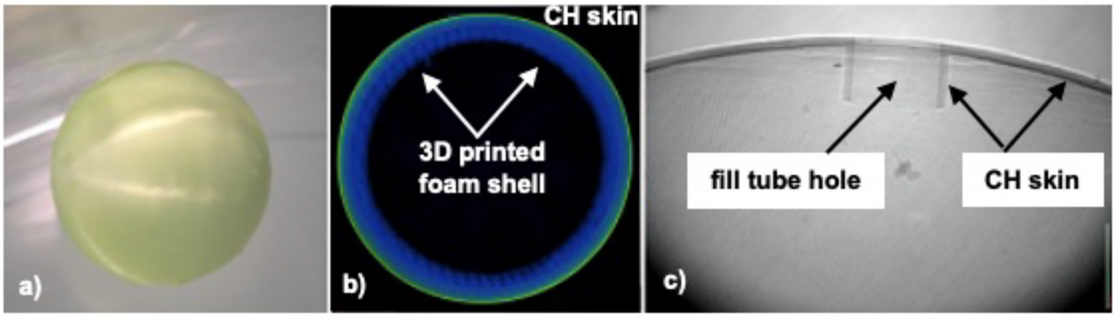

FIG. 4. (a) PDD-WF capsule 3D printed with the dimensions specified in Fig. 1; (b) full diameter tomographic image of the capsule; (c) detail of the fill tube region (images courtesy of Alex Haid, GA).

The implosion trajectory for an example PDD-WF simulation is shown in Fig. 5. In this case, a 1D version of the simulation is compared with the 2D HYDRA simulation. Both simulations use a laser input of 1.4 MJ with a peak power of 230 TW and the pulse shape shown in Fig. 3. The 2D simulation includes details of laser beam spot size, pointing, and cone powers that are not included in the 1D simulation. Even so, the trajectories of the simulations are generally in agreement. It can be seen that the CH skin (shown in red) is completely ablated prior to the end of the foot pulse and that the wetted foam serves as the ablator throughout the main drive pulse. Some key features of the hot blow-off plasma at times of 7 ns, 9 ns, and 11 ns are shown in Fig. 6.

These include laser intensity (TW/cm^2), laser energy deposition (J/μg/ns), electron temperature (keV), and electron density (cm^{-3}). Note that there are significant ($\sim$30%) high spatial frequency modulations in both the laser intensity and the laser absorption in the region beyond the critical radius (located at an electron density of 9×10^{21} cm^{-3}), generated here by the numerics of a finite number of randomly distributed laser rays (300 rays/beam) being absorbed on a finite resolution ($\sim$1° polar angle resolution) hydrodynamic grid. It should not be inferred that these numerics can be equated to the actual noise spectrum on NIF. However, the simulation clearly shows that these laser-driven perturbations are filtered by the significant conduction region between the laser absorption region located beyond the critical surface and the ablation front where the capsule is being driven. Consequently, the residual lower spatial frequencies, whose source is dominated by the summation of the average transverse laser intensity patterns of the individual beams, become the dominate drive asymmetry for this concept and can be adequately modeled with fairly low spatial resolution as shown here. This is a key advantage of low-intensity laser illumination where the drive is dominated not by planar Manheimer ablation, but by strong inverse Bremsstrahlung ablation.[29]

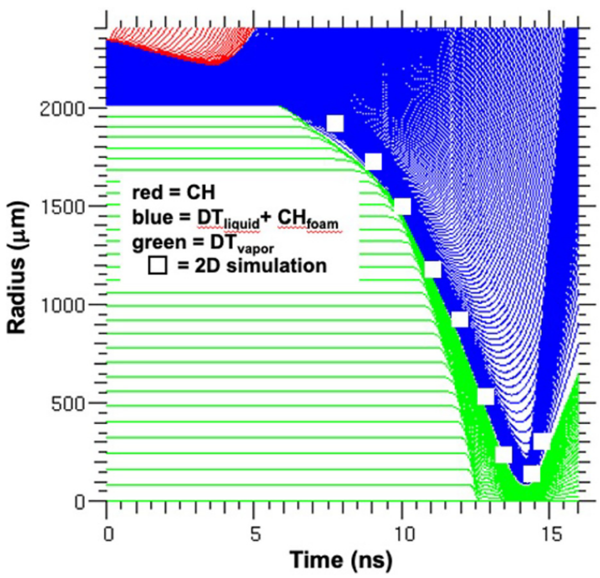

FIG. 5. Comparison of 1D (curves) and 2D (squares) simulated implosion trajectories.

As the laser power increases, the blow-off plasma is important, and significant laser absorption begins to occur at a radius of about 3 mm. Thus, even during the peak of the laser pulse, the laser intensity does not exceed 210 TW/cm^2. Importantly, it should be noted that results from NIF experiments using a similar PDD laser pointing scheme and intensity indicate that laser energy absorption efficiency is very high (>95%) and backscatter measurements $\sim$1% are low,[24] indicating that CBET losses are <5% when the peak laser intensity is kept below 250 TW/cm^2. With the critical surface and the laser energy deposition remaining out at a radius of 2.5–3.0 mm at late times in the implosion, it seems clear that the drive energy is coupled to the imploding shell via electron thermal conductivity. On close examination, it appears that the electron temperature gradients in this gap region are modest, and one might expect that electron thermal flux limiting is not a critical aspect in the simulations. In fact, a series of 2D simulations have been run with electron flux limiters covering the range from 0.03 to 0.10, with very similar implosion behavior and ignition occurring at about the same time in the simulations.

Density contours of the imploding, inner portion of the wetted foam region are shown in Fig. 7 for times of 11 ns, 12 ns, 13 ns, and 14 ns. There are some noticeable angular density fluctuations in the imploding shell. However, in a simulation in which the number of angular zones is doubled, it appears that the fluctuations and mode amplitudes are uncorrelated with zoning. Clearly, the shape of the imploding shell at the end of the laser pulse in this simulation indicates that the pole was driven harder than the equator. Other 2D simulations indicate that the pole/equator shape can be adjusted via changes in the laser cone power fraction. However, even with the significant Legendre P2 mode asymmetry in this simulation, the hot spot ignites. Details of the ignition and thermonuclear burn phases of the simulation are shown in Fig. 8.

At the time of ignition [Fig. 8(a)], the hot spot (region with $5 < T_{ion} < 15$ keV) is quite large compared with a typical high CR indirect drive DT ice layer implosion (hot spot volume $\sim$100X indirect-drive). Within about 20 ps after ignition [Fig. 8(b)], a burn propagation wave heats the dense polar fuel to an ion temperature exceeding 20 keV. At about 80 ps after ignition [Fig. 8(c)], the thermonuclear explosion phase is under way with most of the DT/lattice plasma heated to an ion temperature above 40 keV. The encouraging aspect is that, even with non-ideal symmetry, ignition and a thermonuclear yield of 62 MJ (neutron yield $\sim 2 \times 10^{19}$) are achieved in this PDD-WF simulation. Variations on this 2D HYDRA simulation have yields in the range of 50–100 MJ, depending on beam pointing, meshing, and physics settings. Variations on the re-partitioning of laser ring energy and power can be used to improve the symmetry, but overall thermonuclear yields remain below 100 MJ. The 2D simulation depicted in Figs. 5–8 used an initial vapor density of 1.0 mg/cm^3. A summary of key parameters of the example 2D simulation is provided in Table I. As discussed in Refs. 10, 11, 14, and 17, the same capsule design fielded with higher vapor densities would be more robust to instability growth and mix, but would be expected to have reduced yields with lower hot spot convergence ratios.

IV. SUMMARY, FUTURE WORK, AND CONCLUDING REMARKS

A new approach to ICF ignition and propagating burn is introduced. The concept is referred to as the polar direct drive-wetted foam

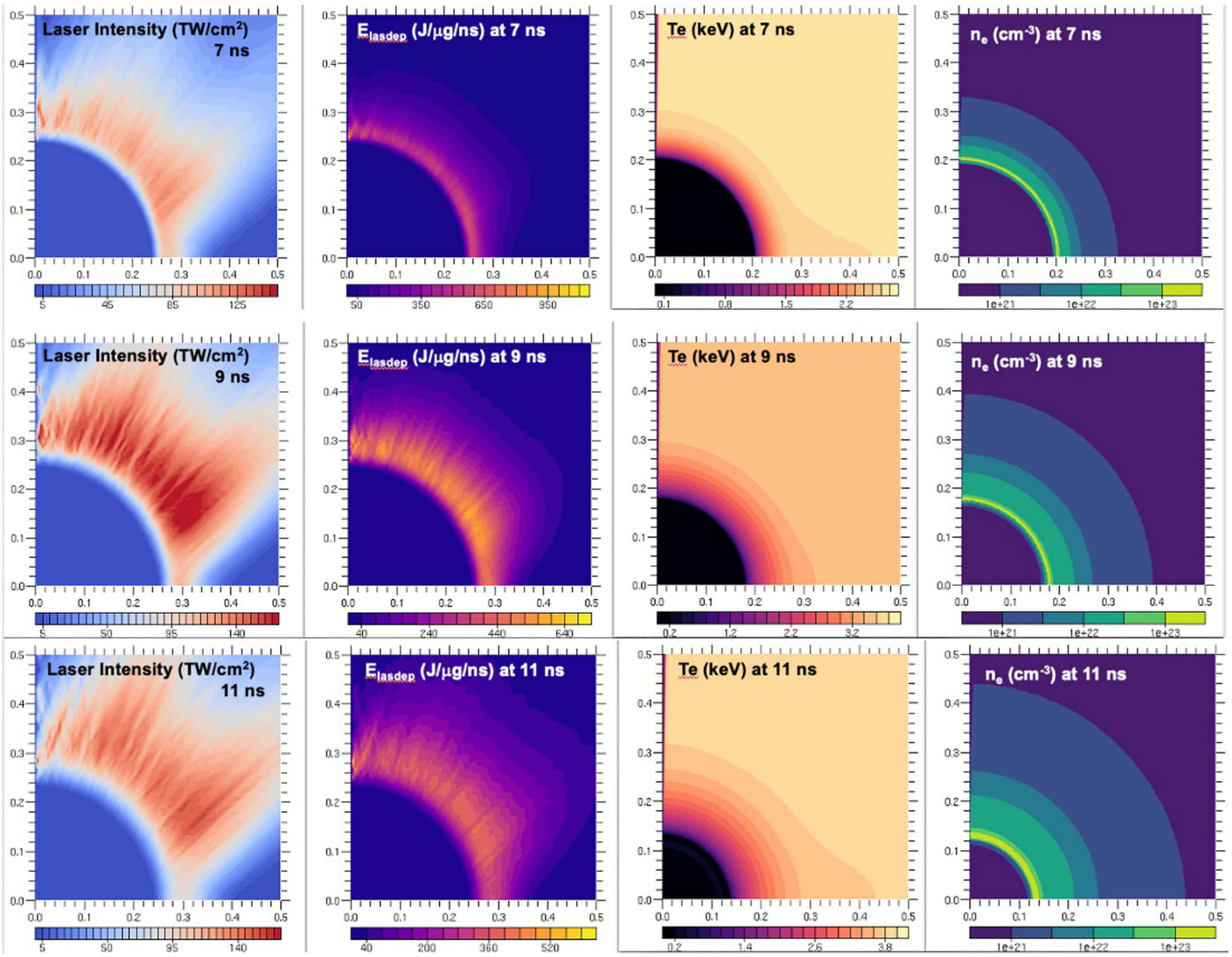

FIG. 6. Contour plots of laser intensity (TW/cm^2), laser deposition (J/μg/ns), electron temperature (keV), and electron density (cm^{-3}) at times of 7 ns, 9 ns, and 11 ns during the laser pulse.

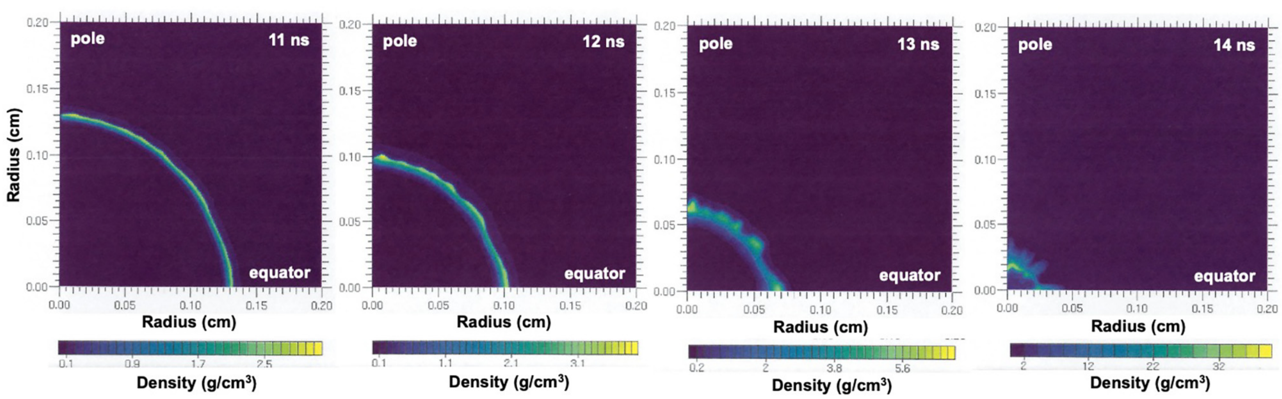

FIG. 7. Density contours at times of 11 ns, 12 ns, 13 ns, and 14 ns during the implosion.

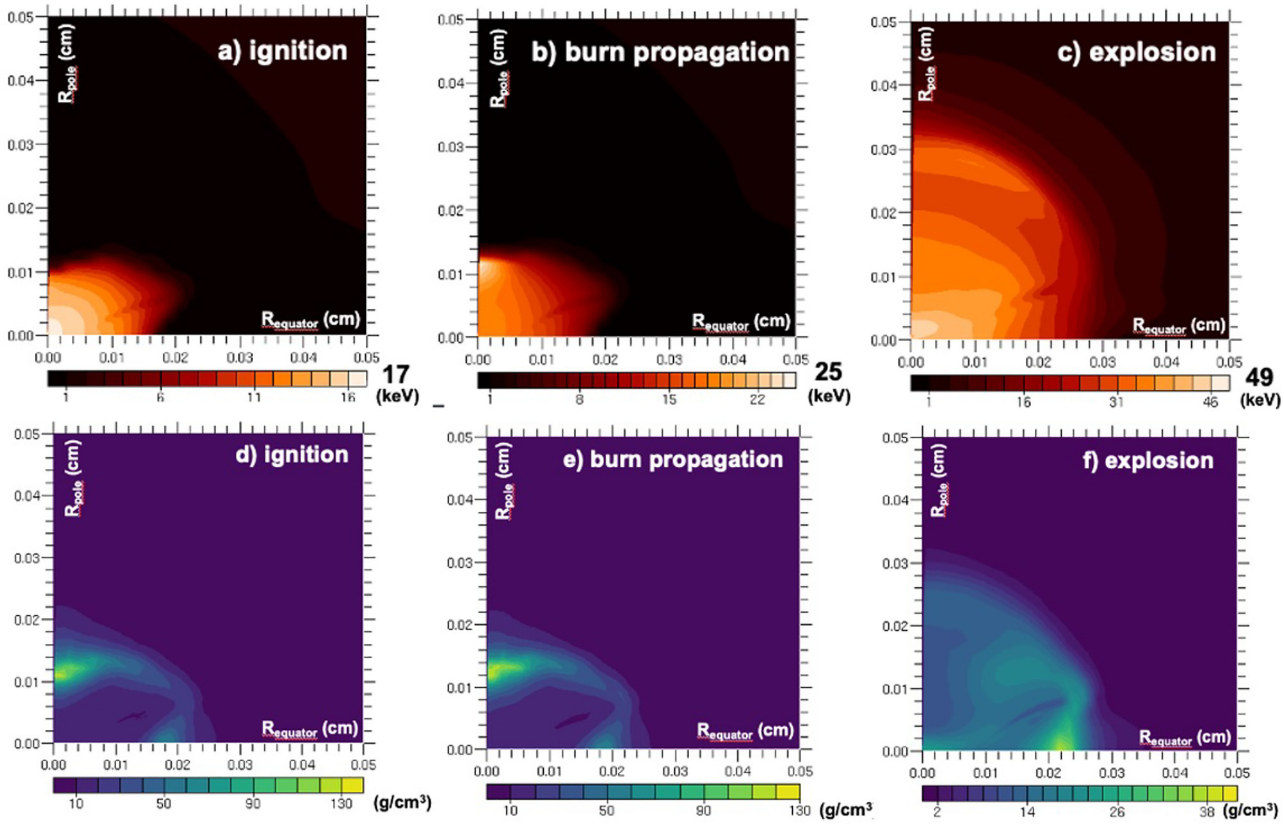

FIG. 8. (a)–(c) Ion temperature and (d–f) density at times of ignition, burn propagation, and thermonuclear explosion, respectively.

(PDD-WF) concept. In this concept, PDD is used to maximize the energy coupling to the capsule, and a thick liquid DT wetted foam shell is used as both the ablator and the fuel layer. A thick liquid DT ablator and a fuel layer are employed to increase hydrodynamic stability through decreased IFAR. The use of DT liquid (instead of DT ice) allows for flexibility in the density of the central DT vapor region, which, in turn, allows for control of the hot spot convergence ratio in a regime that is significantly reduced compared with a DT ice layer implosion. The advantages of reduced convergence implosions to suppress hydrodynamic instabilities and mix are well known, and it is generally acknowledged that the predictive capability of hot spot formation is more robust for a relatively low CR hot spot. An additive manufactured prototype of a PDD-WF capsule has been fabricated using an emergent technology for the one-piece integrated 3D printing of the foam shell, outer skin, and fill tube entrance hole. For future work, we propose that such prototype capsules can be characterized for the levels of imperfections in foam density and thickness uniformity, out-of-roundness, and outer skin roughness. In a feedback process, 2D and 3D simulations can be used to determine tolerances and specifications on these various target imperfections, and to study effects of laser nonuniformities (imprint) and power balance. Off-line cryogenic experiments must be done to explore and understand the liquid DT wetting characteristics of the new type of 3D printed CH lattice class of foams. Appropriate PDD cryogenic capabilities must be demonstrated at NIF. Finally, although it is an old idea, a new interest in the use of wetted foam as an ablator material opens up opportunities for experimental demonstration and characterization of the concept.

With a 1.4 MJ NIF laser input energy, the 2D simulation presented here indicates the potential for thermonuclear yields of up to 50–100 MJ. Thinking ahead to potential inertial fusion energy (IFE) applications,[31–33] an important parameter would be the predicted capsule gain, G, in the range of approximately $35 < G < 70$. Within the IFE community, it has long been thought that the product of driver efficiency, η, and gain is required to be $\eta G > 10$. This assumes that the recycled fraction of the power plant must be less than 25%. Yet, as pointed out by Bodner,[32] the derivation of $\eta G > 10$ is *"rather soft… if instead, it is assumed that society and the economy will accept energy at about three times this minimal cost, the requirement becomes $\eta G > 4$."* It follows, then, that the ηG requirement could change if society decides that it is acceptable to pay more for electricity in order to cut back on the use of fossil fuels to reduce CO_2 emissions. Another consideration is that future driver efficiencies might be quite high. In a recent presentation, Campbell[33] pointed out that advances in diode pumped solid-state lasers might ultimately result in >20% efficient lasers. Thus, the predicted PDD-WF capsule gain might be adequate for IFE. PDD-WF targets have fewer components than indirect drive targets, and presumably, future target fabrication developments will

TABLE I. Key parameters from example 2D simulation of a PDD-WF target.

Parameter	Value	Notes:
Laser energy absorbed	1.44 MJ	99% of the energy in laser pulse
Peak IFAR	18	$R_{a,2/3}$ / $\Delta_{2/3}$, ablation front is at 2/3 of the initial vapor radius and $\Delta_{2/3}$ is taken between the inner and outer positions where the shell density equals the initial density of the ablator[30]
Peak implosion velocity	370 μm/ns	Peak-to-peak in density profile at 12.6 ns and 12.5 ns (mass weighted average of density peaks)
Kinetic energy at V_{peak}	120 kJ	Sum of kinetic energy of all inward-moving zones
Hydrodynamic efficiency	8.3%	Kinetic energy at peak velocity / absorbed laser energy
Fuel adiabat at V_{peak}	7.4	Pressure/cold curve pressure for DT+CH mixed EOS (mass weighted average of peak density zones)
Fuel mass at stagnation	1.68 mg	Mass of unablated DT
Hot spot radius at ignition	135 μm	$(3/4\pi\ V_{hs})^{1/3}$, where V_{hs} = sum of volume of all zones with $T_{ion} > 5.2$ keV
Hot spot CR	15	Initial inner foam shell radius/hot spot radius at ignition
Hot spot mass	161 μg	Sum of the mass of zones with $T_{ion} > 5.2$ keV
Hot spot energy density	51 Gb	Sum of internal energy of $T_{ion} > 5.2$ keV zones / $V_{hs.}$ ($\sim$ 94 kJ of alpha energy has been produced by this time)
Hot spot central pressure	67 Gb	Mass weighted average of initial vapor zones
Effective areal density	1.1 gm/cm^2	Each l-line is assigned an effective ρ and R, where $R = (3/4\pi V)^{1/3}$, and V = sum of zonal volumes
Fuel burn-up fraction	10.7%	Calculated using only the unablated DT mass
Total thermonuclear yield	62 MJ	14 MeV neutron yield of 2.2×10^{19}

also bring costs down. Another aspect to consider is the long-term potential for the rapid mass production of 3D printed PDD-WF capsules. For IFE applications, additive manufacturing of capsules would seem to have advantages over traditional ICF target fabrication techniques.

ACKNOWLEDGMENTS

This work was supported by the Laboratory Directed Research and Development program of Los Alamos National Laboratory under Project No. 20200765ER, Lawrence Livermore National Laboratory under Contract DE-AC52–07NA27344, and General Atomics Internal Research and Development funds.

AUTHOR DECLARATIONS

Conflict of interest

The authors have no conflicts to disclose.

DATA AVAILABILITY

The data that support the findings of this study are available from the corresponding author upon reasonable request.

REFERENCES

1. E. M. Campbell and W. J. Hogan, "The National Ignition Facility – Applications for inertial fusion energy and high-energy-density science," Plasma Phys. Controlled Fusion **41**, B39 (1999).
2. J. Lindl, "Development of the indirect-drive approach to inertial confinement fusion and the target physics basis for ignition and gain," Phys. Plasmas **2**, 3933 (1995).
3. A. B. Zylstra, A. L. Kritcher, O. A. Hurricane, D. A. Callahan, K. Baker, T. Braun, D. T. Casey, D. Clark, K. Clark, T. Döppner, L. Divol, D. E. Hinkel, M. Hohenberger, C. Kong, O. L. Landen, A. Nikroo, A. Pak, P. Patel, J. E. Ralph, N. Rice, R. Tommasini, M. Schoff, M. Stadermann, D. Strozzi, C. Weber, C. Young, C. Wild, R. P. J. Town, and M. J. Edwards, "Record energetics for an inertial fusion implosion at NIF," Phys. Rev. Lett. **126**, 025001 (2021).
4. S. Skupsky, J. A. Marozas, R. S. Craxton, R. Betti, T. J. B. Collins, J. A. Delettrez, V. N. Goncharov, P. W. McKenty, P. B. Radha, T. R. Boehly, J. P. Knauer, F. J. Marshall, D. R. Harding, J. D. Kilkenny, D. D. Meyerhofer, T. C. Sangster, and R. L. McCrory, "Polar direct drive on the National Ignition Facility," Phys. Plasmas **11**, 2763 (2004).
5. R. A. Sacks and D. H. Darling, "Direct drive cryogenic ICF capsules employing DT wetted foam," Nucl. Fusion **27**, 447 (1987).
6. C. B. Yeamans, G. E. Kemp, Z. B. Walters, H. D. Whitley, P. W. McKenty, E. M. Garcia, Y. Yang, R. S. Craxton, and B. E. Blue, "High yield polar direct drive fusion neutron sources at the National Ignition Facility," Nucl. Fusion **61**, 046031 (2021).
7. R. E. Olson, R. J. Leeper, J. L. Kline, A. B. Zylstra, S. A. Yi, J. Biener, T. Braun, B. J. Kozioziemski, J. D. Sater, P. A. Bradley, R. R. Peterson, B. M. Haines, L. Yin, L. F. Berzak Hopkins, N. B. Meezan, C. Walters, M. M. Biener, C. Kong, J. W. Crippen, G. A. Kyrala, R. C. Shah, H. W. Herrmann, D. C. Wilson, A. V. Hamza, A. Nikroo, and S. H. Batha, "First liquid layer inertial confinement fusion implosions at the National Ignition Facility," Phys. Rev. Lett. **117**, 245001 (2016).
8. S. W. Haan, J. D. Lindl, D. A. Callahan, D. Clark, S. J. D. Salmonson, B. A. Hammel, L. J. Atherton, R. C. Cook, M. J. Edwards, S. Glenzer, A. V. Hamza, S. P. Hatchett, M. C. Herrmann, D. E. Hinkel, D. D. Ho, H. Huang, O. S. Jones, J. Kline, G. Kyrala, O. L. Landen, B. J. MacGowan, M. M. Marinak, D. D. Meyerhofer, J. L. Milovich, K. A. Moreno, E. I. Moses, D. H. Munro, A. Nikroo, R. E. Olson, K. Peterson, S. M. Pollaine, J. E. Ralph, H. F. Robey, B. K. Spears, P. T. Springer, L. J. Suter, C. A. Thomas, R. P. Town, R. Vesey, S. V. Weber, H. L. Wilkens, and D. C. Wilson, "Point design targets, specifications,

and requirements for the 2010 ignition campaign on the National Ignition Facility," Phys. Plasmas **18**, 051001 (2011).
[9]R. E. Olson, B. M. Haines, R. R. Peterson, and G. Moses, "Alternative approach to ICF ignition and burn propagation," in Proceedings of 61st Annual Meeting of the APS Division of Plasma Physics, Talk BO4.00011, No. LA-UR-19-30561 (2019).
[10]R. E. Olson, B. M. Haines, C. Di Stefano, H. F. Robey, R. R. Peterson, R. J. Leeper, G. E. Kemp, C. B. Yeamans, and B. E. Blue, "Concept for increased neutron yield and potential ICF ignition at the NIF," in Proceedings of 62nd Annual Meeting APS Division of Plasma Physics, Talk GO09.00005, No. LA-UR-20-28870 (2020).
[11]R. E. Olson, R. J. Leeper, S. A. Yi, J. L. Kline, A. B. Zylstra, R. R. Peterson, R. Shah, T. Braun, J. Biener, B. J. Kozioziemski, J. D. Sater, M. M. Biener, A. V. Hamza, A. Nikroo, L. Berzak Hopkins, D. Ho, S. LePape, and N. B. Meezan, "Wetted foam liquid fuel ICF target experiments," J. Phys. Conf. Ser. **717**, 012042 (2016).
[12]A. B. Zylstra, S. A. Yi, B. M. Haines, R. E. Olson, R. J. Leeper, T. Braun, J. Biener, J. L. Kline, S. H. Batha, L. Berzak Hopkins, S. Bhandarkar, P. A. Bradley, J. Crippen, M. Farrell, D. Fittinghoff, H. W. Herrmann, H. Huang, S. Khan, C. Kong, B. J. Kozioziemski, G. A. Kyrala, T. Ma, N. B. Meezan, F. Merrill, A. Nikroo, R. R. Peterson, N. Rice, J. D. Sater, R. C. Shah, M. Stadermann, P. Volegov, C. Walters, and D. C. Wilson, "Variable convergence liquid layer implosions on the National Ignition Facility," Phys. Plasmas **25**, 056304 (2018).
[13]B. M. Haines, R. E. Olson, W. Sweet, S. A. Yi, A. B. Zylstra, P. A. Bradley, F. Elsner, H. Huang, R. Jimenez, J. L. Kline, C. Kong, G. A. Kyrala, R. J. Leeper, R. Paguio, S. Pajoom, R. R. Peterson, M. Ratledge, and N. Rice, "Robustness to hydrodynamic instabilities in indirectly driven layered capsule implosions," Phys. Plasmas **26**, 012707 (2019).
[14]R. E. Olson and R. J. Leeper, "Alternative hot spot formation techniques using liquid deuterium-tritium layer inertial confinement fusion capsules," Phys. Plasmas **20**, 092705 (2013).
[15]R. W. Paddock, H. Martin, R. T. Ruskov, R. H. H. Scott, W. Garbett, B. M. Haines, A. B. Zylstra, R. Aboushelbaya, M. W. Mayr, B. T. Spiers, R. H. W. Wang, and P. A. Norreys, "One-dimensional hydrodynamic simulations of low convergence ratio direct-drive inertial confinement fusion implosions," Philos. Trans. R. Soc. A **379**, 20200224 (2021).
[16]T. J. B. Collins, J. A. Marozas, R. Betti, D. R. Harding, P. W. McKenty, P. B. Radha, S. Skupsky, V. N. Goncharov, J. P. Knauer, and R. L. McCrory, "One Megajoule wetted foam target design performance for The National Ignition Facility," Phys. Plasmas **14**, 056308 (2007).
[17]B. M. Haines, S. A. Yi, R. E. Olson, S. F. Khan, G. A. Kyrala, A. B. Zylstra, P. A. Bradley, R. R. Peterson, J. L. Kline, R. J. Leeper, and R. C. Shah, "The effects of convergence ratio on the implosion behavior of DT layered inertial confinement fusion capsules," Phys. Plasmas **24**, 072709 (2017).
[18]B. M. Haines, D. S. Clark, C. R. Weber, M. J. Edwards, S. H. Batha, and J. L. Kline, "Cross-code comparison of the impact of the fill tube on high yield implosions on the National Ignition Facility," Phys. Plasmas **27**, 082703 (2020).
[19]R. S. Craxton, K. S. Anderson, T. R. Boehly, V. N. Goncharov, D. R. Harding, J. P. Knauer, R. L. McCrory, P. W. McKenty, D. D. Meyerhofer, J. F. Myatt, A. J. Schmitt, J. D. Sethian, R. W. Short, S. Skupsky, W. Theobald, W. L. Kruer, K. Tanaka, R. Betti, T. J. B. Collins, J. A. Delettrez, S. X. Hu, J. A. Marozas, A. V. Maximov, D. T. Michel, P. B. Radha, S. P. Regan, T. C. Sangster, W. Seka, A. A. Solodov, J. M. Soures, C. Stoeck, and J. D. Zuegel, "Direct-drive inertial confinement fusion: A review," Phys. Plasmas **22**, 110501 (2015).
[20]T. J. B. Collins and J. A. Marozas, "Mitigation of cross-beam energy transfer in ignition-scale polar-direct-drive target designs for the National Ignition Facility," Phys Plasmas **25**, 072706 (2018).
[21]J. A. Marozas, M. Hohenberger, M. J. Rosenberg, D. Turnbull, T. J. B. Collins, P. B. Radha, P. W. McKenty, J. D. Zuegel, F. J. Marshall, S. P. Regan, T. C. Sangster, W. Seka, E. M. Campbell, V. N. Goncharov, M. W. Bowers, J. M. G. Di Nicola, G. Erbert, B. J. MacGowan, L. J. Pelz, and S. T. Yang, "First observation of cross-beam energy transfer mitigation for direct-drive inertial confinement fusion implosions using wavelength detuning at the National Ignition Facility," Phys. Rev. Lett. **120**, 085001 (2018).
[22]T. J. B. Collins, J. A. Marozas, K. S. Anderson, R. Betti, R. S. Craxton, J. A. Delettrez, V. N. Goncharov, D. R. Harding, F. J. Marshall, R. L. McCrory, D. D. Meyerhofer, P. W. McKenty, P. B. Radha, A. Shvydky, S. Skupsky, and J. D. Zuegel, "A polar drive ignition design for the National Ignition Facility," Phys. Plasmas **19**, 056308 (2012).
[23]N. S. Krasheninnikova, M. J. Schmitt, K. Molvig, S. C. Hsu, B. S. Scheiner, D. W. Schmidt, V. Geppert-Kleinrath, P. W. McKenty, D. T. Michel, D. H. Edgell, F. J. Marshall, and H. Huang, "Development of a directly driven multi-shell platform: Laser drive energetics," Phys. Plasmas **27**, 022706 (2020).
[24]M. J. Schmitt, B. S. Scheiner, D. W. Schmidt, L. Kot, M. J. Rosenberg, C. A. Wilde, H. Huang, P. W. McKenty, B. Keenan, and K. Molvig, "First directly-driven double shell implosions at the NIF," in Proceeding of 62nd Annual Meeting APS Division of Plasma Physics, Talk GO09.00009, No. LA-UR-20-29178 (2020).
[25]J. Serbin, A. Ovsianikov, and B. Chichkov, "Fabrication of woodpile structures by two-photon polymerization and investigation of their optical properties," Opt. Exp. **12**, 5221 (2004).
[26]M. Bailly-Grandvaux, D. Kawahito, C. McGuffey, J. Strehlow, B. Edghill, M. S. Wei, N. Alexander, A. Haid, C. Brabetz, V. Bagnoud, R. Hollinger, M. G. Capeluto, J. J. Rocca, and F. N. Beg, "Ion acceleration from microstructured targets irradiated by high-intensity picosecond laser pulses," Phys. Rev. E **102**, 021201 (2020).
[27]D. R. Rusby, P. M. King, A. Pak, N. Lemos, S. Kerr, G. Cochran, I. Pagano, A. Hannasch, H. Quevedo, M. Spinks, M. Donovan, A. Link, A. Kemp, S. C. Wilks, G. J. Williams, M. J.-E. Manuel, Z. Gavin, A. Haid, F. Albert, M. Aufderheide, H. Chen, C. W. Siders, A. Macphee, and A. Mackinnon, "Enhancements in laser-generated hot-electron production via focusing cone targets at short pulse and high contrast," Phys. Rev. E **103**, 053207 (2021).
[28]M. M. Marinak, G. D. Kerbel, N. A. Gentile, O. Jones, D. Munro, S. Pollaine, T. R. Dittrich, and S. W. Haan, "Three-dimensional HYDRA simulations of National Ignition Facility targets," Phys. Plasmas **8**, 2275 (2001).
[29]B. Scheiner and M. Schmitt, "Considerations for the modeling of the laser ablation region of ICF targets with Lagrangian simulations," AIP Adv. **11**, 105208 (2021).
[30]V. N. Goncharov, T. C. Sangster, R. Betti, T. R. Boehly, M. J. Bonino, T. J. B. Collins, R. S. Craxton, J. A. Delettrez, D. H. Edgell, R. Epstein, R. K. Follett, C. J. Forrest, D. H. Froula, V. Yu. Glebov, D. R. Harding, R. J. Henchen, S. X. Hu, I. V. Igumenshchev, R. Janezic, J. H. Kelly, T. J. Kessler, T. Z. Kosc, S. J. Loucks, J. A. Marozas, F. J. Marshall, A. V. Maximov, R. L. McCrory, P. W. McKenty, D. D. Meyerhofer, D. T. Michel, J. F. Myatt, R. Nora, P. B. Radha, S. P. Regan, W. Seka, W. T. Shmayda, R. W. Short, A. Shvydky, S. Skupsky, C. Stoeckl, B. Yaakobi, J. A. Frenje, M. Gatu-Johnson, R. D. Petrasso, and D. T. Casey, "Improving the hot-spot pressure and demonstrating ignition hydrodynamic equivalence in cryogenic deuterium–tritium implosions on OMEGA," Phys. Plasmas **21**, 056315 (2014).
[31]P. A. Norreys, L. Ceurvorst, J. D. Sadler, B. T. Spiers, R. Aboushelbaya, M. W. Mayr, R. Paddock, N. Ratan, A. F. Savin, R. H. W. Wang, K. Glize, R. M. G. M. Trines, R. Bingham, M. P. Hill, N. Sircombe, M. Ramsay, P. Allan, L. Hobbs, S. James, J. Skidmore, J. Fyrth, J. Luis, E. Floyd, C. Brown, B. M. Haines, R. E. Olson, S. A. Yi, A. B. Zylstra, K. Flippo, P. A. Bradley, R. R. Peterson, J. L. Kline, and R. J. Leeper, "Preparations for a European R&D roadmap for an inertial fusion demo reactor," Philos. Trans. R. Soc. A **379**, 20200005 (2021).
[32]S. E. Bodner, "Critical elements of high gain laser fusion," J. Fusion Energy **1**, 221 (1981).
[33]E. M. Campbell, "Inertial fusion energy: Opportunities and challenges," Second Annual LaserNetUS Meeting (2021).